Type I interferon enhances necroptosis of *Salmonella* Typhimurium–infected macrophages by impairing antioxidative stress responses

Nina Judith Hos,[1,2,3,5]* Raja Ganesan,[1,3]* Saray Gutiérrez,[1,3] Deniz Hos,[2,4] Jennifer Klimek,[1] Zeinab Abdullah,[6] Martin Krönke,[1,2,3,5] and Nirmal Robinson[1,3]

[1]Cluster of Excellence in Cellular Stress Responses in Aging-Associated Diseases and [2]Center for Molecular Medicine Cologne, University of Cologne, Cologne, Germany
[3]Institute for Medical Microbiology, Immunology and Hygiene and [4]Department of Ophthalmology, University Hospital Cologne, Cologne, Germany
[5]German Center for Infection Research (DZIF), Partner Site Cologne-Bonn, Germany
[6]Institute of Experimental Immunology, University of Bonn, Bonn, Germany

Salmonella enterica serovar Typhimurium exploits the host's type I interferon (IFN-I) response to induce receptor-interacting protein (RIP) kinase–mediated necroptosis in macrophages. However, the events that drive necroptosis execution downstream of IFN-I and RIP signaling remain elusive. In this study, we demonstrate that *S.* Typhimurium infection causes IFN-I–mediated up-regulation of the mitochondrial phosphatase Pgam5 through RIP3. Pgam5 subsequently interacts with Nrf2, which sequesters Nrf2 in the cytosol, thereby repressing the transcription of Nrf2-dependent antioxidative genes. The impaired ability to respond to *S.* Typhimurium–induced oxidative stress results in reactive oxygen species–mediated mitochondrial damage, energy depletion, transient induction of autophagy, and autophagic degradation of p62. Reduced p62 levels impair interaction of p62 with Keap1, which further decreases Nrf2 function and antioxidative responses to *S.* Typhimurium infection, eventually leading to cell death. Collectively, we identify impaired Nrf2-dependent redox homeostasis as an important mechanism that promotes cell death downstream of IFN-I and RIP3 signaling in *S.* Typhimurium–infected macrophages.

Introduction

Salmonella enterica serovar Typhimurium (*S.* Typhimurium) is a Gram-negative, facultative intracellular pathogen that has evolved several strategies to evade the host's immune defense. One key virulence strategy used by *S.* Typhimurium is the induction of cell death in macrophages (Lindgren et al., 1996). We have previously demonstrated that *S.* Typhimurium exploits the host's type I IFN (IFN-I) response to eliminate macrophages by inducing receptor-interacting protein (RIP) 1– and RIP3-mediated necroptosis (Robinson et al., 2012). Therefore, IFN-I receptor–deficient mice (*Ifnar1*$^{-/-}$) showed enhanced survival after *S.* Typhimurium infection compared with WT mice. Importantly, enhanced control of *S.* Typhimurium in *Ifnar1*$^{-/-}$ mice is specifically mediated by macrophages (Robinson et al., 2012). Although the pathways leading to necrosome formation have been well characterized, the mechanisms downstream of IFN-I/RIP3 leading to necroptosis execution largely remain unknown.

Previous studies have shown that mitochondria play a crucial role in several cell death modalities (Galluzzi et al., 2012). In response to infection, mitochondria can change from a source of energy into organelles that promote cell death by releasing mitochondrial reactive oxygen species (ROS [mtROS]) and toxic proteins that are usually retained within the mitochondrial intermembrane space (Kroemer et al., 2007). As mitochondria are the main producers of ATP, mitochondrial damage drastically impairs cellular energy homeostasis. Consequently, cells increase glycolysis and initiate autophagy to maintain their metabolic demands (Deretic et al., 2013; Kelly and O'Neill, 2015). Autophagy is a highly conserved catabolic process by which large intracellular components, such as protein aggregates and long-lived or damaged organelles, are engulfed into double-membrane vesicles called autophagosomes, which are subsequently degraded by the lysosomal pathway (Mizushima et al., 2008; Deretic et al., 2013). The adapter protein Sqstm1/p62 (hereafter p62) interacts with the autophagosome-localizing protein LC3 and polyubiquitinated cargo, thereby targeting proteins and organelles for autophagosomal degradation (Bjørkøy et al., 2005; Pankiv et al., 2007; Itakura and Mizushima, 2011). Because lipidated LC3 and p62 are degraded by autophagy

*N.J. Hos and R. Ganesan contributed equally to this paper.

Correspondence to Nirmal Robinson: nirmal.robinson@uk-koeln.de

Abbreviations used: ARE, antioxidant response element; BMDM, bone marrow–derived macrophage; mtROS, mitochondrial ROS; OCR, oxygen consumption rate; p.i., post infection; RIP, receptor-interacting protein; RIPA, radioimmunoprecipitation assay; ROS, reactive oxygen species; TMRM, tetramethylrhodamine methyl ester.

The Rockefeller University Press
J. Cell Biol. Vol. 216 No. 12 4107–4121
https://doi.org/10.1083/jcb.201701107

themselves, their protein levels are reciprocally associated with autophagic activity.

Beyond its function as an autophagic adapter protein, p62 also regulates the Keap1–Nrf2 pathway, which has been recognized as a critical regulator of cellular redox homeostasis. Under resting conditions, Keap1 sequesters the transcription factor Nrf2 in the cytoplasm, where it is ubiquitinated and degraded via the proteasomal pathway (Kobayashi et al., 2004; Zhang et al., 2004). Upon oxidative stress, however, p62 interacts with the Nrf2-binding site of Keap1, thus disrupting Nrf2–Keap1 interaction (Komatsu et al., 2010; Lau et al., 2010; Ichimura et al., 2013). Nrf2 is subsequently stabilized and translocated to the nucleus, where it binds to conserved antioxidant response elements (AREs) in the promoter regions of target genes, such as the detoxification enzyme NADPH quinone oxidoreductase 1 (*Nqo1*), the glutathione synthesis enzyme glutamate cysteine ligase (catalytic subunit *Gclc*), and the cell stress protein heme oxygenase-1 (*Hmox-1*; Rushmore et al., 1991; Wasserman and Fahl, 1997; Ishii et al., 2002). In addition, Nrf2 activation is regulated by the mitochondrial phosphatase Pgam5, which has originally been identified as a protein bound to Keap1 (Lo and Hannink, 2006). Besides regulating antioxidative stress responses, Pgam5 has recently been implicated to mediate necroptotic death pathways. Upon TNF-induced necroptosis, Pgam5 is recruited to RIP1- and RIP3-containing protein complexes at the outer mitochondrial membrane, where Pgam5 induces Drp1-mediated mitochondrial fragmentation, resulting in necroptotic cell death (Wang et al., 2012).

In this study, we sought to identify the mechanisms that sensitize macrophages to IFN-I–mediated cell death upon *S*. Typhimurium infection. We report here that IFN-I/RIP3-mediated up-regulation of Pgam5 sequesters Nrf2 in the cytosol and impairs the transcription of Nrf2-dependent antioxidative genes. Diminished antioxidative response results in ROS-mediated mitochondrial damage, energy depletion, and transient induction of autophagy. Autophagy posttranscriptionally down-regulates p62, leading to perturbed p62–Keap1 interaction, which further represses Nrf2 function. Our findings demonstrate that IFN-I signaling critically impairs Nrf2-mediated redox homeostasis during *S*. Typhimurium infection, which sensitizes macrophages to cell death.

Results

IFN-I signaling exacerbates *S*. Typhimurium–induced mitochondrial damage

Mitochondrial dysfunction has been identified as a major cause for cell death (Galluzzi et al., 2012). We therefore investigated whether *S*. Typhimurium infection causes mitochondrial damage in macrophages and whether this is regulated by IFN-I signaling. Using confocal microscopy, we assessed mitochondrial morphology in uninfected and *S*. Typhimurium–infected bone marrow–derived macrophages (BMDMs) from WT and *Ifnar1*$^{-/-}$ mice. In contrast to uninfected BMDMs, which showed the typical tubular mitochondrial network, WT and *Ifnar1*$^{-/-}$ BMDMs infected with *S*. Typhimurium for 6 h displayed increased mitochondrial fragmentation, indicative of damaged mitochondria (Fig. 1 A). Compared with WT BMDMs, however, the integrity of the mitochondrial network appeared better conserved in infected *Ifnar1*$^{-/-}$ BMDMs. Consistently, electron microscopy revealed an accumulation of damaged mitochondria in *S*. Typhimurium–infected WT BMDMs, whereas mitochondrial integrity was less disrupted in *Ifnar1*$^{-/-}$ BMDMs (Fig. 1 B). Enhanced mitochondrial damage in WT BMDMs correlated with increased mtROS production and decreased mitochondrial membrane potential (ψm), whereas *Ifnar1*$^{-/-}$ BMDMs generated less mtROS in response to *S*. Typhimurium infection, consistent with sustained ψm (Fig. 1, C–E). We additionally assessed mitochondrial function upon *S*. Typhimurium infection by analyzing the oxygen consumption rate (OCR) in BMDMs and found that OCR was reduced more in infected WT BMDMs compared with *Ifnar1*$^{-/-}$ BMDMs (Fig. S1). Furthermore, mitochondrial mass was distinctly decreased in WT BMDMs 6 h after infection, whereas it was enhanced in *Ifnar1*$^{-/-}$ BMDMs (Fig. 1, F and G). As expected, ATP levels declined in both WT and *Ifnar1*$^{-/-}$ BMDMs after 2 and 6 h of *S*. Typhimurium infection (Fig. 1 H). However, ATP levels remained significantly higher in infected *Ifnar1*$^{-/-}$ BMDMs compared with WT controls. These findings suggest that *S*. Typhimurium infection causes IFN-I–mediated mitochondrial damage and energy depletion in macrophages.

Mitochondrial damage results in the transient induction of autophagy

Under starvation conditions, autophagy is triggered to provide energy by recycling cellular organelles and protein aggregates through lysosomal degradation (Mizushima et al., 2008; Deretic et al., 2013). Having shown that *S*. Typhimurium infection causes mitochondrial damage that results in energy depletion, we next investigated whether this induces autophagy. Indeed, we observed that *S*. Typhimurium infection induced the formation of autophagosomes in both WT and *Ifnar1*$^{-/-}$ BMDMs (Fig. 2 A). To assess autophagic activity, we measured expression levels of autophagosome-associated LC3-II (lipidated form) and the autophagic adapter protein p62 in WT and *Ifnar1*$^{-/-}$ BMDMs infected with *S*. Typhimurium. LC3-II and p62 were degraded by the autolysosome themselves, and their amounts were inversely correlated with autophagic flux. As shown in Fig. 2 B, *S*. Typhimurium infection transiently induced autophagy in WT BMDMs (2 h post infection [p.i.]), whereas it was attenuated after 4 and 6 h of infection, as indicated by reduced LC3-I to -II conversion and increased p62 levels. However, autophagic flux was constantly reduced after *S*. Typhimurium infection in *Ifnar1*$^{-/-}$ BMDMs, as shown by a low LC3-II/LC3-I ratio and a strong accumulation of p62 (4 and 6 h p.i.; Fig. 2, C and D). Similarly, neutralization of secreted IFN-β markedly induced accumulation of p62 in WT BMDMs upon *S*. Typhimurium infection, which was comparable to the amount of p62 in autophagy-deficient *Atg7*$^{-/-}$ BMDMs (Fig. S2 A). Consistent with reduced autophagic activity, relative mRNA levels of *Lc3b* (LC3) and *Lamp1*, a central indicator of lysosomal biogenesis, were also decreased in infected *Ifnar1*$^{-/-}$ BMDMs compared with WT controls (Fig. 2, E and F). Of note, *Ifnar1*$^{-/-}$ BMDMs were not generally deficient in autophagy because LC3-I to -II conversion was induced upon Torin1 treatment (Fig. S2 B). Furthermore, differential autophagy in WT and *Ifnar1*$^{-/-}$ BMDMs was not caused by altered mTOR activation, as shown by similar phosphorylation levels of p70 S6 kinase (Fig. S2 B), and did not have a significant effect on bacterial burden (Fig. S2 C). These results indicate that IFN-I signaling transiently triggers autophagy in *S*. Typhimurium–infected macrophages (2 h p.i.), whereas autophagy is inhibited during the later course of infection (4 and 6 h p.i.), leading to elevated p62 levels.

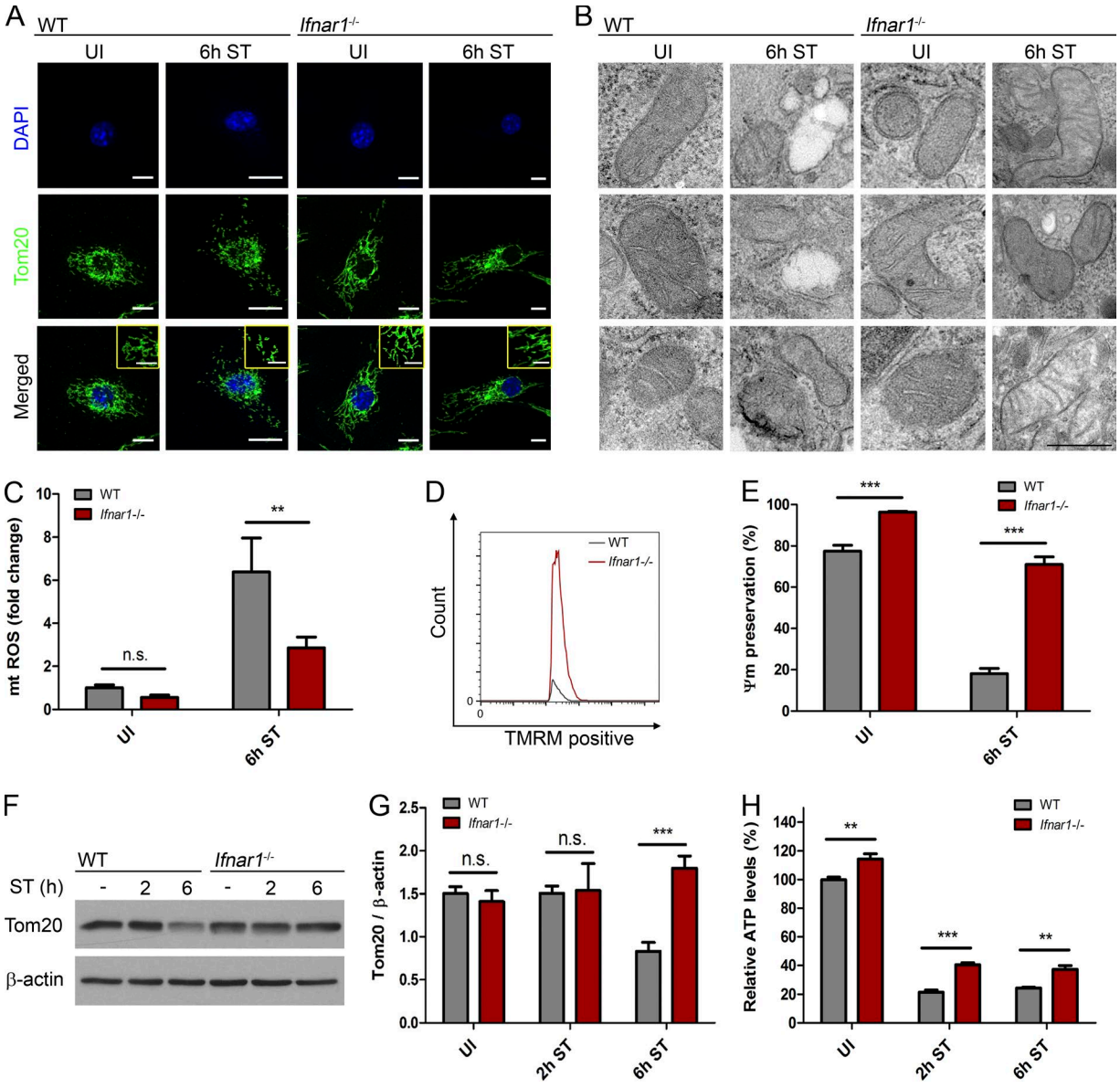

Figure 1. **IFN-I signaling exacerbates *S.* Typhimurium–induced mitochondrial damage.** (A) Immunofluorescence staining of mitochondrial network. WT and *Ifnar1*$^{-/-}$ BMDMs were infected with *S.* Typhimurium for the indicated time, immunostained for Tom20, and examined by confocal microscopy. Each inset represents a magnified image. Bars: (main images) 10 µm; (insets) 4 µm. (B) Electron micrographs of mitochondria in uninfected and *S.* Typhimurium–infected WT and *Ifnar1*$^{-/-}$ BMDMs. Shown are three representative examples of mitochondria in uninfected or *S.* Typhimurium–infected WT and *Ifnar1*$^{-/-}$ BMDMs. Bar, 250 nm. (C) Relative mtROS. WT and *Ifnar1*$^{-/-}$ BMDMs were infected with *S.* Typhimurium for the indicated time, and the amounts of mtROS relative to uninfected WT BMDMs were analyzed by FACS using MitoSOX staining. Data are representative of two independent experiments performed in triplicate. (D and E) Flow cytometric analysis for ψm. (D) WT and *Ifnar1*$^{-/-}$ BMDMs were infected with *S.* Typhimurium for 6 h, and the number of TMRM-positive cells was measured by flow cytometry. Damaged mitochondria failed to sequester TMRM, resulting in the loss of fluorescence intensity. (E) Relative changes in ψm of uninfected and *S.* Typhimurium–infected WT and *Ifnar1*$^{-/-}$ BMDMs were analyzed by TMRM fluorescence. Data are representative of three independent experiments performed in triplicate. (F and G) Immunoblot analysis of mitochondrial mass. (F) Uninfected or *S.* Typhimurium–infected WT and *Ifnar1*$^{-/-}$ BMDMs were immunostained for Tom20 as a marker for mitochondrial mass. (G) Densitometric quantification of Tom20 expression from three independent experiments. (H) Luminescence analysis of relative ATP levels. WT and *Ifnar1*$^{-/-}$ BMDMs were infected with *S.* Typhimurium for the indicated time, and the luminescence signal was measured to determine ATP levels. Values were normalized to ATP levels of uninfected WT BMDMs. The assay was repeated three times and was performed in quintuplicates. Results are shown as means ± SD. ST, *S.* Typhimurium. UI, uninfected. **, P < 0.01; ***, P < 0.001. n.s., not significant.

p62 levels contribute to IFN-I–mediated cell death upon *S.* Typhimurium infection

In autophagy-deficient cells, p62 regulates the formation of cytoplasmic inclusion bodies in response to oxidative stress (Komatsu et al., 2007). Furthermore, p62-positive protein aggregates are characteristic features of neurodegenerative and chronic liver diseases (Zatloukal et al., 2002; Umemura et al., 2016). To investigate whether p62-positive protein aggregates also occur in infected macrophages, we performed confocal microscopy on WT and *Ifnar1*$^{-/-}$ BMDMs 6 h after *S.* Typhimurium infection. Consistent with our immunoblot data, *S.* Typhimurium infection enhanced p62 expression in WT BMDMs, and p62 strongly accumulated in infected *Ifnar1*$^{-/-}$ BMDMs (Fig. 3, A and B). A moderate up-regulation of *Sqstm1* (the gene encoding p62)

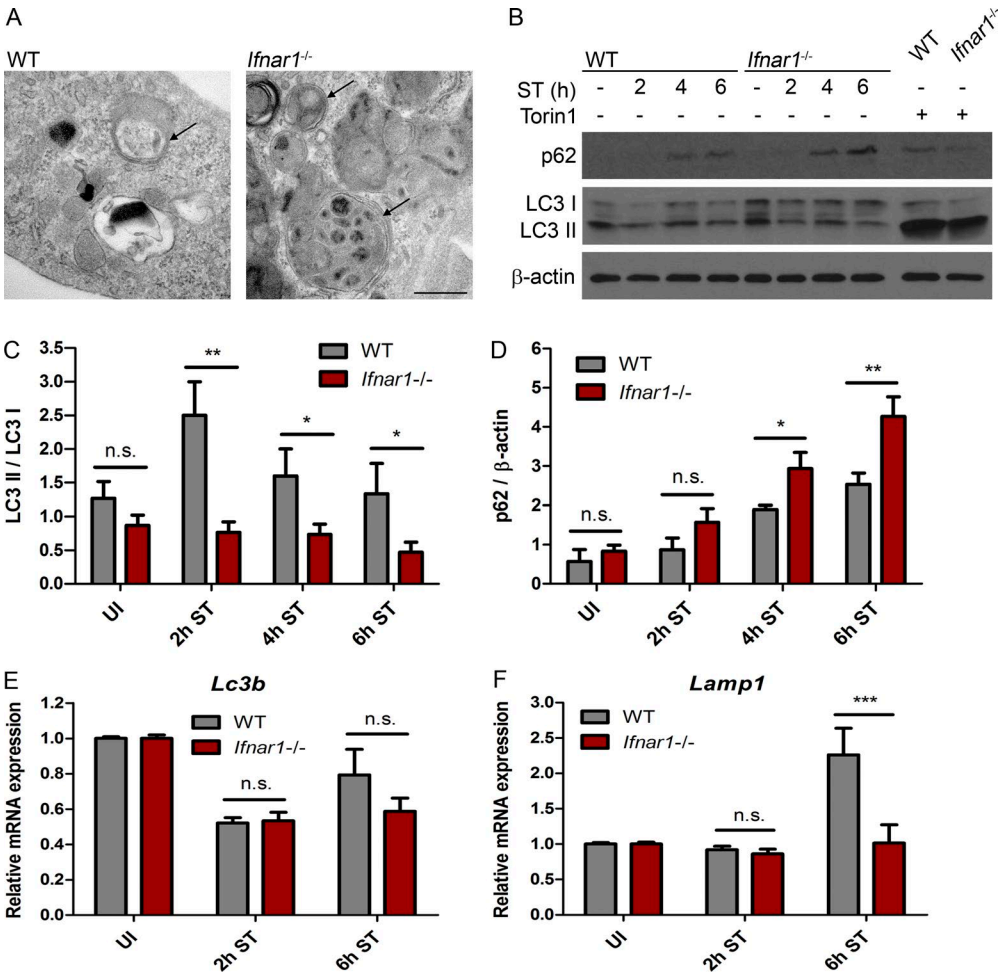

Figure 2. **Mitochondrial damage results in the transient induction of autophagy.** (A) Electron micrographs of autophagosomes in *S.* Typhimurium–infected WT and *Ifnar1*$^{-/-}$ BMDMs (2 h p.i.). Arrows point to double-membrane structures indicative of autophagosomes. Bar, 500 nm. (B–D) Immunoblot analysis of autophagy marker proteins. WT and *Ifnar1*$^{-/-}$ BMDMs were infected with *S.* Typhimurium for the indicated time or treated with 10 µM Torin1 (4 h) and then immunoblotted for p62 and LC3 (B). LC3-I to LC3-II conversion rates (C) and p62 expression levels (D) were determined by densitometric quantification. Torin1 inhibits mTOR and was used as a positive control for autophagy induction. Data represent three independent experiments. (E and F) Relative *Lc3b* and *Lamp1* mRNA expression. WT and *Ifnar1*$^{-/-}$ BMDMs were infected with *S.* Typhimurium for the indicated time, and *Lc3b* (E) and *Lamp1* mRNA (F) expression were determined by real-time PCR. Values were normalized to the amounts of mRNA in uninfected BMDMs. Data are means ± SD from two independent experiments with three replicates each. ST, *S.* Typhimurium. UI, uninfected. *, P < 0.05; **, P < 0.01; ***, P < 0.001. n.s., not significant.

mRNA was also observed in infected *Ifnar1*$^{-/-}$ BMDMs compared with WT controls (Fig. 3 C). Moreover, we found that p62 assembled on large protein aggregates (≥1 µm) in the perinuclear region (Fig. 3 A). We therefore reasoned that p62 accumulation in *Ifnar1*$^{-/-}$ BMDMs is caused by impaired autophagic degradation. Accordingly, treatment of infected WT and *Ifnar1*$^{-/-}$ BMDMs with Concanamycin A, which inhibits lysosomal acidification and degradation, further elevated p62 levels compared with untreated controls (Fig. 3, D and E). We next determined the importance of elevated p62 levels for macrophage survival using either control or *Sqstm1*/p62-specific siRNA (Fig. 3 F). As expected, *S.* Typhimurium induced more cell death in WT BMDMs compared with *Ifnar1*$^{-/-}$ BMDMs (Fig. 3 G). Knockdown of p62 significantly reduced cell viability in both WT and *Ifnar1*$^{-/-}$ BMDMs (Fig. 3 G). Importantly, autophagy-deficient *Atg7*$^{-/-}$ BMDMs survived even less than WT BMDMs, whereas neutralization of IFN-β protected WT and *Atg7*$^{-/-}$ BMDMs from *S.* Typhimurium–induced cell death (Fig. S3). We therefore conclude that IFN-I mediates cell death upon *S.* Typhimurium infection independent of autophagy but dependent on p62.

IFN-I signaling attenuates Nrf2 activation and antioxidative stress responses during *S.* Typhimurium infection

Previous work on autophagy-deficient hepatocytes and epithelial kidney cells suggested that p62 accumulation induces antioxidative stress responses by interacting with the Nrf2-binding site on Keap1 (Komatsu et al., 2010; Lau et al., 2010). Nrf2 is subsequently stabilized and translocated to the nucleus, where it promotes the expression of numerous detoxifying enzymes and cytoprotective proteins (Komatsu et al., 2010; Lau et al., 2010; Ichimura et al., 2013). As p62 strongly accumulated in *Ifnar1*$^{-/-}$ BMDMs upon *S.* Typhimurium infection, we investigated whether this correlated with increased Nrf2 activation. In *Ifnar1*$^{-/-}$ BMDMs, Nrf2 protein expression was markedly enhanced after 2, 4, and 6 h of *S.* Typhimurium infection compared with WT BMDMs, whereas Keap1 expression was decreased 6 h p.i. (Fig. 4, A–C). Furthermore, p62 strongly colocalized with Keap1 in infected *Ifnar1*$^{-/-}$ BMDMs (Fig. 4, D and E). As a consequence of increased p62–Keap1 interaction, significantly

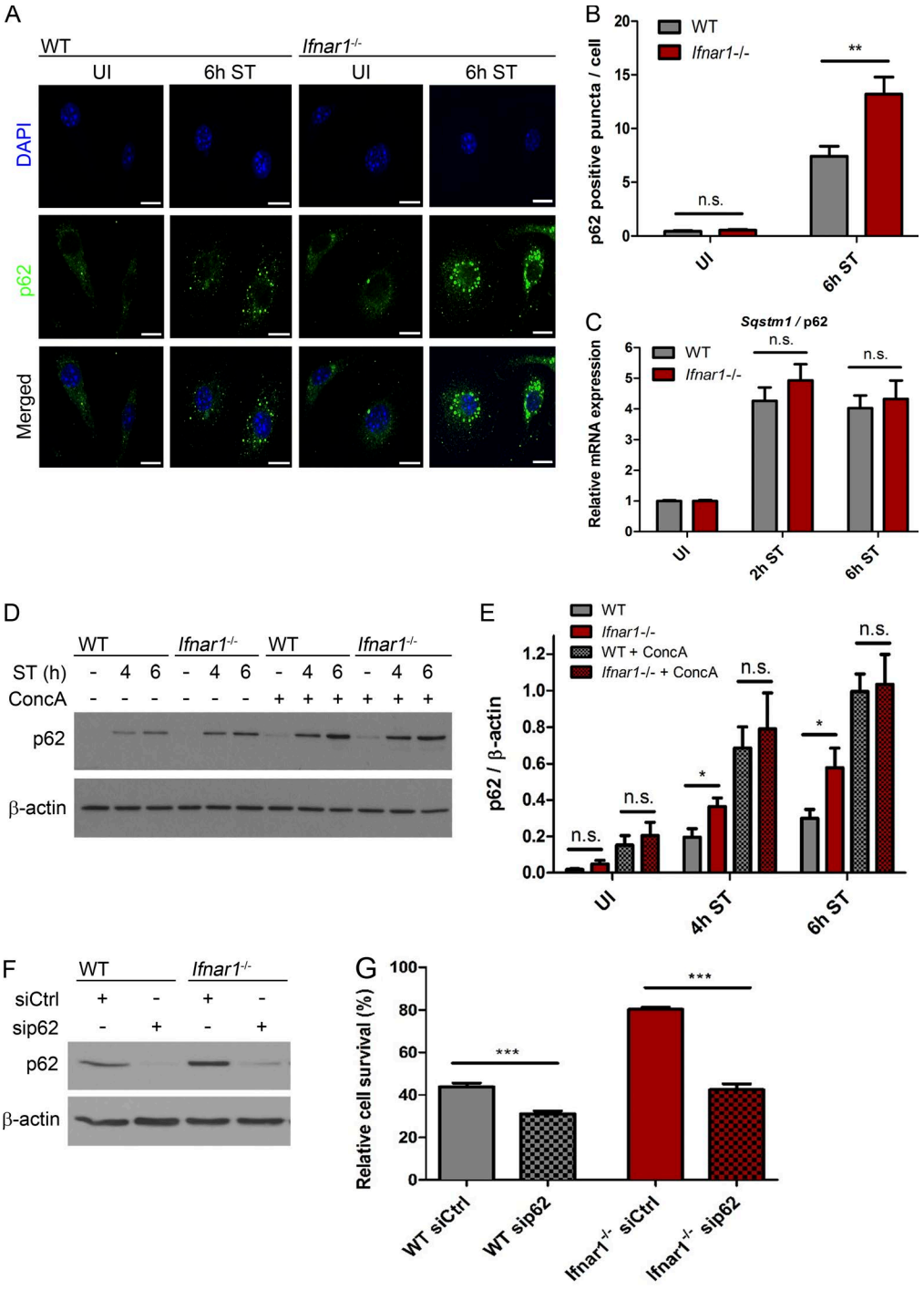

Figure 3. **p62 levels contribute to IFN-I–mediated cell death upon *S.* Typhimurium infection.** (A and B) Immunofluorescence staining of p62. After infection with *S.* Typhimurium, WT and *Ifnar1*$^{-/-}$ BMDMs were immunostained for p62 (A), and the number of p62-positive puncta per cell was quantified (B). $n = 50$ cells each, repeated three times. Bars, 10 µm. (C) Relative *Sqstm1* mRNA expression. WT and *Ifnar1*$^{-/-}$ BMDMs were infected with *S.* Typhimurium for the indicated time, and *Sqstm1* (the gene encoding p62) mRNA expression was determined by real-time PCR. Values were normalized to the amounts of mRNA in uninfected BMDMs. Two independent experiments with three replicates each. (D and E) Immunoblot analysis of autophagic flux. WT and *Ifnar1*$^{-/-}$ BMDMs were either infected with *S.* Typhimurium or pretreated with Concanamycin A (ConcA; 100 nM, 2 h) and then infected with *S.* Typhimurium in the presence of 50 nM Concanamycin A for the indicated time. Samples were immunoblotted for p62 (D), and p62 expression from three independent experiments was quantified densitometrically (E). Concanamycin A inhibits lysosomal acidification of the autophagosome and is used to determine autophagic flux. ST, *S.* Typhimurium. UI, uninfected. (F) Immunoblot analysis of p62 knockdown efficiency. WT and *Ifnar1*$^{-/-}$ BMDMs were transfected with nontargeting (siCtrl) or siRNA specific for *Sqstm1*/p62 (sip62). Thereafter, total cell lysates were analyzed for p62 by Western blotting. (G) Luminescence analysis of p62-dependent cell death. Luminescence signals of WT and *Ifnar1*$^{-/-}$ BMDMs transfected with nontargeting (siCtrl) or *Sqstm1*/*p62*-specific (sip62) siRNA were assessed to determine cell viability 6 h after *S.* Typhimurium infection. Values were normalized to the luminescence signal of uninfected WT BMDMs. Results are representative of three independent experiments performed in quintuplicates and are shown as means ± SD. *, $P < 0.05$; **, $P < 0.01$; ***, $P < 0.001$. n.s., not significant.

more Nrf2 translocated into the nucleus in *S*. Typhimurium–infected *Ifnar1*$^{-/-}$ BMDMs compared with WT BMDMs (Fig. 4, F–H). Consistently, relative mRNA expression levels of Nrf2 target genes, such as *Nqo1, Hmox-1*, and *Gclc*, were significantly up-regulated in *Ifnar1*$^{-/-}$ BMDMs compared with WT BMDMs (Fig. 4, I–K). To confirm that the up-regulation of *Nqo1*, *Hmox-1*, and *Gclc* in *Ifnar1*$^{-/-}$ BMDMs is mediated by p62, we transfected *Ifnar1*$^{-/-}$ BMDMs with control or anti-*Sqstm1*/p62 siRNA (Fig. S4 A) and determined expression levels of these genes. As shown in Fig. S4 (B–D), genetic silencing of *Sqstm1*/p62 significantly reduced *Nqo1*, *Hmox-1*, and *Gclc* expression. Importantly, loss of Atg7 had no significant effect on Nrf2-dependent gene expression unless IFN-β was neutralized (Fig. S4, E and F), indicating that p62 expression, but not autophagy deficiency, is critical for antioxidative stress responses. Collectively, our results demonstrate that *S*. Typhimurium–induced IFN-I interferes with p62–Keap1 interaction and reduces Nrf2-regulated cytoprotective gene expression.

Impaired Nrf2 function mediates *S*. Typhimurium–induced cell death

We next analyzed whether the reduced ability to respond to pathogen-induced oxidative stress sensitizes WT BMDMs to cell death. For this purpose, we transfected WT and *Ifnar1*$^{-/-}$ BMDMs with siRNA against *Nfe2l2* (the gene encoding Nrf2). Knockdown of Nrf2 was confirmed by immunoblot analysis (Fig. 5 A). In line with our previous findings, *S*. Typhimurium infection induced significantly less cell death in *Ifnar1*$^{-/-}$ BMDMs compared with WT controls (Fig. 5 B). Nrf2 deficiency had no significant effect on cell death in WT BMDMs. However, Nrf2-deficient *Ifnar1*$^{-/-}$ BMDMs were more susceptible to *S*. Typhimurium–induced cell death than *Ifnar1*$^{-/-}$ transfected with control siRNA. In fact, cell death in Nrf2-deficient *Ifnar1*$^{-/-}$ BMDMs was comparable to the level of cell death in Nrf2-deficient WT BMDMs (Fig. 5 B), indicating that increased survival of *Ifnar1*$^{-/-}$ BMDMs was mediated by Nrf2. Similarly, pharmacological inhibition of Nrf2 using trigonelline significantly increased cell death in infected *Ifnar1*$^{-/-}$ BMDMs compared with untreated controls, whereas the effect of Nrf2 inhibition on cell death was less pronounced in infected WT BMDMs (Fig. 5 C). In contrast, pharmacological activation of Nrf2 by Bardoxolone methyl (CDDO) markedly increased WT viability after *S*. Typhimurium infection, whereas CDDO had no additional effect on infected *Ifnar1*$^{-/-}$ BMDMs (Fig. 5 C). We confirmed that Nrf2 function is critical for cellular redox homeostasis upon *S*. Typhimurium infection because knockdown of Nrf2 further enhanced mtROS production in WT and *Ifnar1*$^{-/-}$ BMDMs compared with controls (Fig. 5 D). Because we observed that increased antioxidative responses provide resistance to *S*. Typhimurium–induced cell death, we surmised that scavenging mtROS could be cytoprotective. Therefore, we specifically quenched mtROS in *S*. Typhimurium–infected WT BMDMs using mitoTEMPO, which significantly improved cell survival compared with untreated controls (Fig. 5 E). Collectively, these results indicate that disturbed redox homeostasis caused by *S*. Typhimurium infection is an important trigger for cell death in macrophages. In particular, *S*. Typhimurium–induced IFN-I impairs Nrf2 activation, which sensitizes infected macrophages to cell death.

Nrf2 function upon *S*. Typhimurium infection is regulated by RIP3

We have previously shown that *S*. Typhimurium exploits IFN-I signaling to induce RIP1- and RIP3-mediated necroptosis in macrophages (Robinson et al., 2012). Because RIP kinases act downstream of the IFN-I receptor, we speculated that RIP kinases are also involved in regulating Nrf2 function. As shown in Fig. 6 A, *S*. Typhimurium infection induced the phosphorylation of RIP3 in an IFN-I–dependent manner. Furthermore, *S*. Typhimurium infection promoted MLKL phosphorylation, a downstream target of RIP3 kinase, which was reduced in the absence of IFN-I signaling (Fig. 6 A). Consistently, loss of RIP3 remarkably reduced phosphorylation of MLKL (Fig. 6 B). As *S*. Typhimurium infection induced more IL-1β secretion in *Ifnar1*$^{-/-}$ BMDMs compared with WT BMDMs, we excluded pyroptosis as the predominant type of cell death mediated by IFN-I signaling (Fig. S5, A and B). Similar to *Ifnar1*$^{-/-}$ BMDMs, *RIP3*$^{-/-}$ BMDMs showed accumulation of p62, reduced Keap1, and increased Nrf2 expression upon infection with *S*. Typhimurium (Fig. 6 C). We detected more Nrf2 in the nucleus of infected *RIP3*$^{-/-}$ BMDMs compared with WT BMDMs (Fig. 6, D and E), and loss of RIP3 significantly up-regulated *Nqo1* and *Gclc* expression (Fig. 6, F and G). These results collectively indicate that upon *S*. Typhimurium infection IFN-I activates RIP3, which subsequently impairs Nrf2 nuclear translocation and transcription of Nrf2-dependent antioxidative genes.

Pgam5 prevents Nrf2 activation downstream of IFN-I/RIP3

We next sought to identify the mechanism by which IFN-I/RIP3 impairs Nrf2 function. Upon TNF-induced necrosis, MLKL has been reported to mediate the interaction of RIP1- and RIP3-containing protein complexes with the mitochondrial phosphatase Pgam5 (Wang et al., 2012). Subsequently, Pgam5 is targeted to the outer membrane of mitochondria, where it forms a ternary complex with Nrf2 and Keap1 in which Keap1 bridges Pgam5 and Nrf2 (Lo and Hannink, 2008). We therefore investigated whether Pgam5 function is regulated by IFN-I/RIP3 signaling and whether Pgam5 impacts on Nrf2-mediated antioxidative stress responses to *S*. Typhimurium infection. *S*. Typhimurium infection induced the expression of Pgam5 in WT, *Ifnar1*$^{-/-}$, and *RIP3*$^{-/-}$ BMDMs. However, Pgam5 expression was reduced in *Ifnar1*$^{-/-}$ and *RIP3*$^{-/-}$ BMDMs (Fig. 7, A and B). To investigate whether Pgam5 interacts with Nrf2, anti-Nrf2 immunoprecipitates of WT, *Ifnar1*$^{-/-}$, and *RIP3*$^{-/-}$ BMDMs were subjected to immunoblot analysis. Pgam5 strongly coimmunoprecipitated with Nrf2 in WT BMDMs 6 h after *S*. Typhimurium infection, whereas Pgam5 was not detectable in anti-Nrf2 immunoprecipitates of *Ifnar1*$^{-/-}$ and *RIP3*$^{-/-}$ BMDMs (Fig. 7, C and D), suggesting that IFN-I/RIP3 promotes a protein complex comprising Pgam5 and Nrf2. We next transfected WT BMDMs with anti-Pgam5 siRNA to analyze whether Pgam5 regulates Nrf2 activation and function. Knockdown of Pgam5 was confirmed by immunoblot analysis (Fig. 7 E). Interestingly, genetic silencing of Pgam5 enhanced nuclear translocation of Nrf2 (Fig. 7 F) and transcription of Nrf2-dependent *Nqo1* (Fig. 7 G). Collectively, IFN-I signaling upon *S*. Typhimurium infection enhances Pgam5–Nrf2 interaction via RIP3, which critically impairs Nrf2 function.

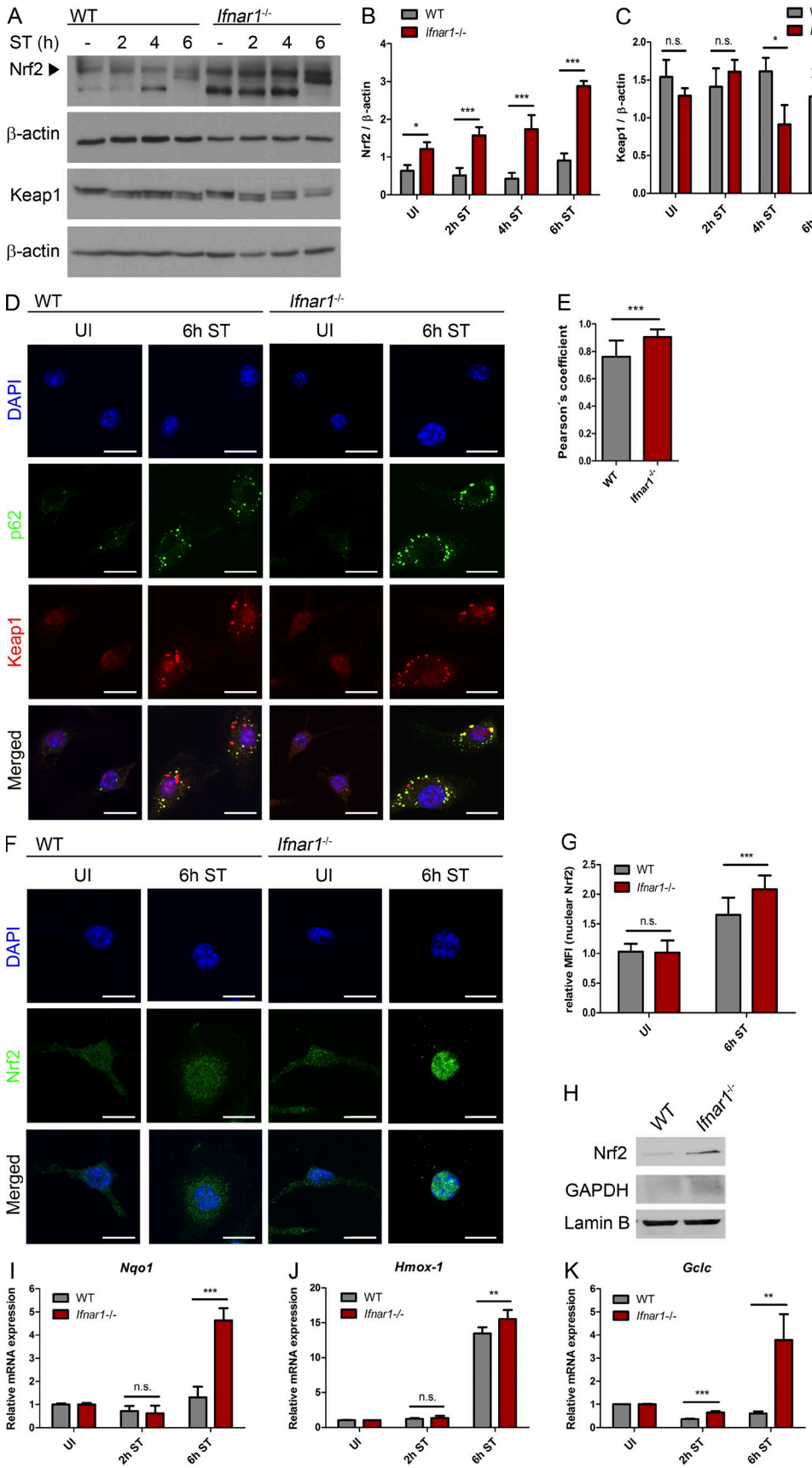

Figure 4. **IFN-I signaling attenuates Nrf2 activation and antioxidative stress responses during *S.* Typhimurium infection.** (A–C) Immunoblot analysis of Nrf2 and Keap1. After *S.* Typhimurium infection, total cell lysates of WT and *Ifnar1*$^{-/-}$ BMDMs were immunoblotted (A) and densitometrically quantified for Nrf2 (B) and Keap1 expression (C). Data are representative of three independent experiments. (D and E) Immunofluorescence staining of subcellular distribution

Discussion

We report here that IFN-I signaling impairs Nrf2-dependent antioxidative stress responses to *S*. Typhimurium infection, which results in ROS-mediated mitochondrial dysfunction and subsequent cell death. We specifically show that *S*. Typhimurium–induced IFN-I activates RIP3, which promotes the expression of the mitochondrial phosphatase Pgam5 and its complex formation with Nrf2. Enhanced Pgam5–Nrf2 interaction attenuates nuclear translocation of Nrf2 and the transcription of Nrf2-dependent antioxidative genes. The impaired ability of macrophages to respond to *S*. Typhimurium–induced oxidative stress leads to ROS-mediated mitochondrial damage and energy depletion, which transiently triggers autophagy and reduces p62 levels. IFN-I perturbs the interaction of p62 with Keap1, thereby further down-regulating Nrf2-dependent antioxidative genes, eventually sensitizing infected macrophages to cell death.

Mitochondria are key organelles that provide most of the cellular ATP, but they have also been recognized as important mediators of innate immune signaling and programmed cell death (Wasilewski and Scorrano, 2009; Chandel, 2014; Weinberg et al., 2015). Therefore, disruption of mitochondrial integrity has been identified as a key virulence strategy of both viral and bacterial pathogens (Arnoult et al., 2009; Stavru et al., 2011). Furthermore, IFN-I has been shown to inhibit mitochondrial function and ATP production, which might contribute to the antiproliferative effect of IFN-I (Lewis et al., 1996). Here, we demonstrate that *S*. Typhimurium infection induces mitochondrial damage in macrophages, which results in decreased ATP levels. Of note, IFN-I signaling further enhances mitochondrial damage and ROS production caused by RIP3-mediated repression of Nrf2 function. As a consequence of mitochondrial dysfunction, infected macrophages transiently induce autophagy to preserve energy homeostasis, whereas autophagy is triggered to a much lower extent in the absence of IFN-I signaling. Similarly, recent work has shown that IFN-I treatment induced autophagy in multiple cancer cell lines. This effect was mediated by inhibition of mTOR, a master regulator of autophagy (Schmeisser et al., 2013). In contrast, in our study, mTOR is activated shortly after *S*. Typhimurium infection, which occurs independent of IFN-I. A recent study also reported that mTOR was activated during *S*. Typhimurium infection, resulting in the blockade of autophagy (Owen et al., 2014). In line with this observation, we also found that autophagy is inhibited at later stages of infection and that loss of IFN-I signaling further attenuates autophagy. In addition, we have recently demonstrated that *S*. Typhimurium actively inhibits autophagy by *Salmonella* pathogenicity island 2 (SPI-2)–encoded effector proteins (Ganesan et al., 2017).

Autophagy defects are relevant to human diseases, mainly through the accumulation of p62-positive protein aggregates (Komatsu et al., 2007). Because p62 is degraded along with polyubiquitinated cargo by autophagy, accumulation of this protein is indicative of defective autophagic flux. p62 is also a component of cytosolic inclusion bodies (Zatloukal et al., 2002), as they can be found in neurodegenerative disorders, such as Parkinson's and Alzheimer's disease (Hara et al., 2006; Komatsu et al., 2006; Rubinsztein, 2006), chronic liver inflammation (Denk et al., 2006; Stumptner et al., 2007), and various cancer entities (Thompson et al., 2003; Mathew et al., 2009; Inami et al., 2011; Umemura et al., 2016). In our study, p62 expression is increased in macrophages after *S*. Typhimurium infection both on mRNA and protein levels. We observed the formation of p62-containing protein aggregates in infected macrophages, which strongly accumulate in the absence of IFN-I signaling. Although *Sqstm1*/p62 mRNA expression is marginally higher in infected *Ifnar1*$^{-/-}$ BMDMs compared with WT BMDMs, transcriptional up-regulation of *Sqstm1*/p62 mRNA alone cannot explain the increased formation of p62 protein aggregates in *Ifnar1*$^{-/-}$ BMDMs. In fact, the formation of p62-positive aggregates in our study was caused by reduced autophagolysosomal proteolysis of p62, which is in line with the recent results published by Umemura et al. (2016). Our finding that IFN-I signaling reduces p62 is supported by a recent study from Ejlerskov et al. (2015), who also observed accumulation of p62 in IFN-β–deficient neuronal cells.

Elevated p62 levels have been shown to induce the expression of antioxidant enzymes in hepatocytes (Umemura et al., 2016). The Nrf2–Keap1 pathway is a major regulator of antioxidative stress responses, and p62 is known to activate this pathway by suppressing Keap1–Nrf2 interaction. Nrf2 is subsequently stabilized and translocated to the nucleus, where it induces the expression of cytoprotective enzymes (Komatsu et al., 2010; Lau et al., 2010; Ichimura et al., 2013). Furthermore, the importance of the Nrf2 antioxidative pathway has recently been demonstrated for dengue virus infection (Olagnier et al., 2014). In accordance with our findings, the expression of Nrf2-dependent target genes limited ROS production, whereas genetic silencing of *Nrf2* enhanced ROS production and dengue-induced cell death. Genetic silencing of *Nrf2* increased IFN-β mRNA expression upon dengue virus infection. In that particular study, however, the effect of IFN-β on regulating Nrf2-dependent redox homeostasis or cell death has not been addressed. Ichimura et al. (2013) reported that *S*. Typhimurium infection enhanced the expression of Nrf2-dependent cytoprotective genes in mouse embryonic fibroblasts. Another study from the same group suggested that *S*. Typhimurium activates the Keap1–Nrf2 system through phosphorylation of p62 at Ser351 during xenophagy (Ishimura et al., 2014). Accordingly, we found that *S*. Typhimurium infection induces p62 expression and interaction of p62 with Keap1, which is further increased in *Ifnar1*$^{-/-}$ macrophages. However, increased expression of p62 in WT macrophages is not sufficient to promote Nrf2-dependent cytoprotective response. Eventually, IFN-I–mediated repression of Nrf2-dependent genes sensitizes WT

of p62 and Keap1. (D) WT and *Ifnar1*$^{-/-}$ BMDMs were infected with *S*. Typhimurium for the indicated time, immunostained for p62 or Keap1, and examined by confocal microscopy. (E) Pearson correlation coefficient was used to assess p62 and Keap1 colocalization. (F and G) Immunofluorescence staining and quantification of nuclear Nrf2. (F) After *S*. Typhimurium infection, WT and *Ifnar1*$^{-/-}$ BMDMs were immunostained for Nrf2 and examined by confocal microscopy. Bars, 10 µm. (G) Mean fluorescence intensity (MFI) of nuclear Nrf2 was measured using densitometric quantification. $n = 50$ cells each, repeated three times. (H) Immunoblot analysis of nuclear Nrf2. Nuclear fractions of WT and *Ifnar1*$^{-/-}$ BMDMs were prepared 6 h after *S*. Typhimurium infection and were subjected to immunoblot analysis for Nrf2 expression. Lamin B and GAPDH were used as controls. Immunoblots are representative of three independent experiments. (I–K) Relative mRNA expression of Nrf2 downstream target genes. Relative mRNA expression levels of *Nqo1* (I), *Hmox-1* (J), and *Gclc* (K) in *S*. Typhimurium–infected WT and *Ifnar1*$^{-/-}$ BMDMs were determined by real-time PCR. Values were normalized to the amounts of mRNA in uninfected BMDMs. Data are means ± SD from three independent experiments with three replicates each. ST, *S*. Typhimurium. UI, uninfected. *, $P < 0.05$; **, $P < 0.01$; ***, $P < 0.001$. n.s., not significant.

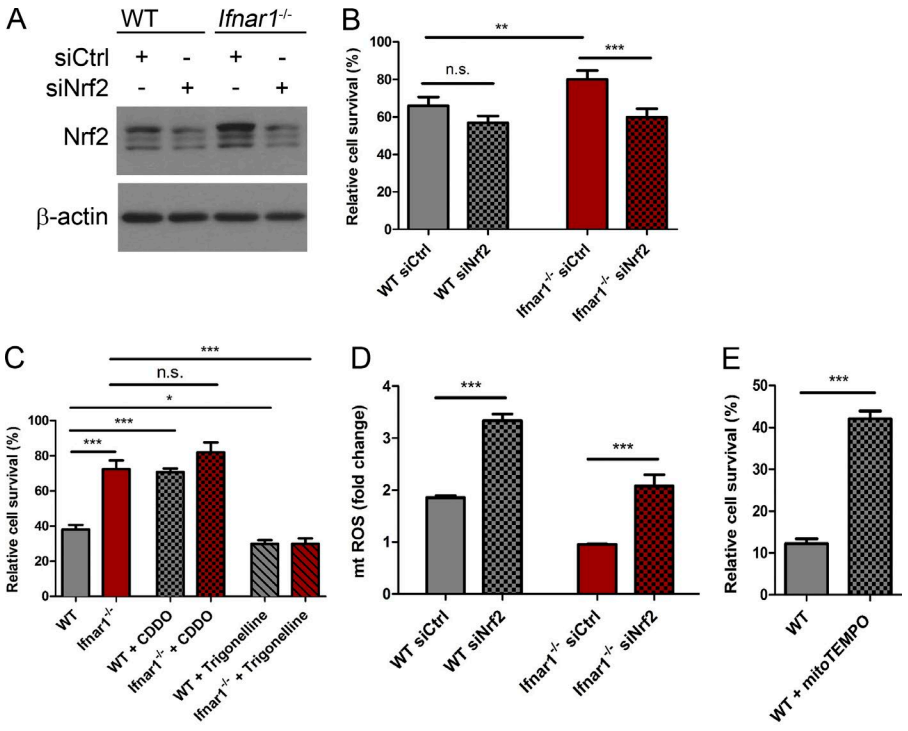

Figure 5. **Impaired Nrf2 function mediates *S.* Typhimurium–induced cell death.** (A) Immunoblot analysis of Nrf2 knockdown efficiency. WT and *Ifnar1*$^{-/-}$ BMDMs were transfected with nontargeting (siCtrl) or siRNA specific for *Nfe2l2* (siNrf2). Thereafter, total cell lysates were analyzed by Western blot for Nrf2. (B) Luminescence analysis of Nrf2-dependent cell death. Luminescence signals of WT and *Ifnar1*$^{-/-}$ BMDMs transfected with nontargeting (siCtrl) or siRNA specific for *Nfe2l2* (siNrf2) were assessed to determine cell viability upon infection with *S.* Typhimurium (6 h p.i.). Values were normalized to the luminescence signal of uninfected WT BMDMs. (C) Luminescence analysis of cell death upon pharmacological modulation of Nrf2 function. Luminescent signals of WT and *Ifnar1*$^{-/-}$ BMDMs treated with the Nrf2 activator CDDO (500 nM for 6 h) or with the Nrf2 inhibitor Trigonelline (100 µM for 6 h) were determined, and cell viability 6 h after *S.* Typhimurium infection was analyzed. Values were normalized to the luminescence signal of uninfected, untreated WT BMDMs. (B and C) Results are representative of three independent experiments performed in quintuplicates and are shown as means ± SD. (D) Nrf2-dependent mtROS. WT and *Ifnar1*$^{-/-}$ BMDMs were transfected with nontargeting (siCtrl) or siRNA specific for *Nfe2l2* (siNrf2) as described in A. Transfected BMDMs were infected with *S.* Typhimurium for 6 h, and the amounts of mtROS relative to uninfected WT siCtrl BMDMs were analyzed by FACS using MitoSOX staining. Data are representative of three independent experiments performed in triplicates. (E) Luminescence analysis of ROS-dependent cell death. Luminescence signals of WT BMDMs with or without mitoTEMPO treatment (100 µM for 6 h) were analyzed to determine cell viability upon *S.* Typhimurium infection (6 h p.i.). Values were normalized to the luminescence signal of uninfected, untreated BMDMs. Results are representative of two independent experiments performed in triplicates and are shown as means ± SD. *, $P < 0.05$; **, $P < 0.01$; ***, $P < 0.001$. n.s., not significant.

macrophages to *S.* Typhimurium–induced cell death. Consistently, the pharmacological activation of Nrf2/ARE genes prevents *S.* Typhimurium–induced cell death in WT macrophages, whereas it has no additional effect in IFN-I–deficient macrophages, where Nrf2 target genes are already highly up-regulated. Discrepancies in previous studies could be attributed to the different cell types investigated, as the response to IFN-I upon *S.* Typhimurium infection possibly differs in the mouse embryonic fibroblasts used by Ichimura et al. (2013). We also observed increased p62 levels in autophagy-deficient *Atg7*$^{-/-}$ macrophages infected with *S.* Typhimurium. However, loss of Atg7 does not result in enhanced Nrf2/ARE gene expression and macrophage survival unless IFN-I signaling is blocked. Although these results suggest that p62 contributes to the regulation of antioxidative responses and macrophage viability upon *S.* Typhimurium infection, additional pathways besides autophagy must be involved in regulating IFN-I–induced cell death.

Importantly, we report here that IFN-I signaling additionally impairs the Nrf2 response to *S.* Typhimurium through the activation of RIP3 and Pgam5. The mitochondrial phosphatase Pgam5 has been identified to form a ternary complex with Nrf2 and Keap1 at the outer mitochondrial membrane in which Keap1 simultaneously binds both Pgam5 and Nrf2 (Lo and Hannink, 2008). Furthermore, Pgam5 has also been implicated to regulate RIP1- and RIP3-induced necroptosis through Drp1-mediated mitochondrial fragmentation (Wang et al., 2012). Our present results indicate that Pgam5 is also critically involved in mediating Nrf2 function in *S.* Typhimurium–infected macrophages. During *S.* Typhimurium infection, IFN-I activates RIP3, resulting in subsequent Pgam5 expression. We found that IFN-I/RIP3 enhances the interaction of Pgam5 with Nrf2 (presumably through Keap1), which sequesters Nrf2 in the cytosol and thereby represses the transcription of antioxidative genes. Similarly, Lo and Hannink (2008) reported that Pgam5 contributed to the repression of Nrf2-dependent ARE genes in HeLa cells.

Cell death induced by pathogens is complex, as multiple players, such as Caspase-1 and -11, are also known to play a significant role (Thurston et al., 2016; Man et al., 2017). Our results demonstrate that IFN-I–regulated cell death is independent of Caspase-1 because IFN-I signaling reduces IL-1β secretion upon *S.* Typhimurium infection. However, it remains to be investigated whether Caspase-11 is an additional player in IFN-I–regulated necroptosis in *S.* Typhimurium–infected macrophages, as IFN-I–induced GTPases are known to regulate Caspase-11 activation (Meunier et al., 2014).

In conclusion, we have unraveled that perturbed cellular redox homeostasis is an important trigger for *S.* Typhimurium–induced cell death. We propose a model in which IFN-I/RIP3 signaling diminishes Nrf2-mediated antioxidative stress responses to *S.* Typhimurium infection through enhanced interaction of Nrf2 with Pgam5 (Fig. 8). The reduced ability to respond to *S.* Typhimurium–induced oxidative stress results in ROS-mediated mitochondrial damage, energy depletion, and the transient induction of autophagy. Autophagy posttranscriptionally down-regulates p62, leading to perturbed p62–Keap1 interaction, which further represses Nrf2 function and eventually sensitizes macrophages to *S.* Typhimurium–induced necroptosis. This implies that targeting IFN-I signaling pathways could provide therapeutic opportunities to treat infection-related pathologies.

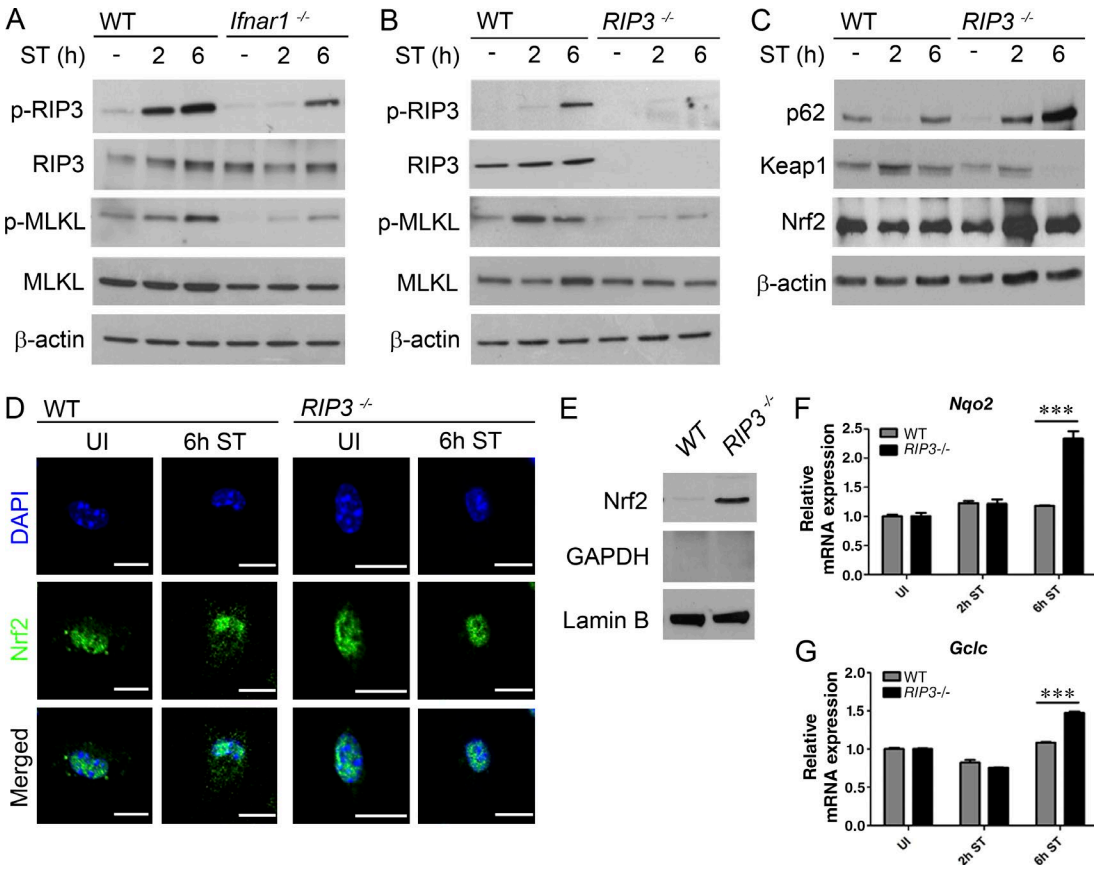

Figure 6. **Nrf2 activation upon *S.* Typhimurium infection is regulated by RIP3.** (A and B) Immunoblot analysis of necrosome activation. After *S.* Typhimurium infection, total cell lysates of WT and *Ifnar1*$^{-/-}$ (A) or WT and *RIP3*$^{-/-}$ BMDMs (B) were subjected to immunoblot analysis with antibodies against RIP3, phospho-RIP3 (p-RIP3), MLKL, and phospho-MLKL (p-MLKL) as markers for necroptotic pathway activation. (C) Immunoblot analysis of p62, Keap1, and Nrf2. Expression levels of p62, Keap1, and Nrf2 were analyzed by immunoblot in total cell lysates of *S.* Typhimurium–infected WT and *RIP3*$^{-/-}$ BMDMs. (A–C) Immunoblots are representative of three independent experiments. (D) Immunofluorescence staining of nuclear Nrf2. After 6 h of *S.* Typhimurium infection, WT and *RIP3*$^{-/-}$ BMDMs were immunostained for Nrf2, and subcellular localization of Nrf2 was examined by confocal microscopy. Bars, 10 µm. (E) Immunoblot analysis of nuclear Nrf2. Nuclear fractions of WT and *RIP3*$^{-/-}$ BMDMs were prepared 6 h after *S.* Typhimurium infection and were subjected to immunoblot analysis for Nrf2 expression. Lamin B and GAPDH were used as controls. Results are representative of three independent experiments. (F and G) RIP3-dependent expression of Nrf2 target genes. Relative mRNA expression levels of *Nqo1* (F) and *Gclc* (G) in *S.* Typhimurium–infected WT and *RIP3*$^{-/-}$ BMDMs were determined by real-time PCR. Values were normalized to the amounts of mRNA in uninfected BMDMs. Data are means ± SD from three independent experiments with three replicates each. ST, *S.* Typhimurium. UI, uninfected. ***, $P < 0.001$.

Materials and methods

Mice and generation of BMDMs

Bone marrow from C57BL/6 WT, IFN-I receptor (*Ifnar1*$^{-/-}$), autophagy-related protein 7 (*Atg7*$^{-/-}$; provided by M. Schramm, University of Cologne, Cologne, Germany), and receptor-interacting serine/threonine–protein kinase 3 (*RIP3*$^{-/-}$)–deficient mice (provided by M. Pasparakis, University of Cologne, and V. Dixit, Genentech, San Francisco, CA) was differentiated into macrophages in RPMI medium (FG1415; Millipore) containing 10% FBS (10270-106; Thermo Fisher Scientific) supplemented with 20% L929 cell culture supernatant for 7 d. Nonadherent cells were removed on days 3 and 5, and adherent BMDMs were used from day 7 to 9. All animal studies were performed according to institutional guidelines on animal welfare and were approved by the North Rhine-Westphalian State Agency for Nature, Environment, and Consumer Protection (Landesamt für Natur, Umwelt, and Verbraucherschutz Nordrhein-Westfalen; file no: 84–02.05.40.14.082 and 84-02.04.2015.A443) and the local animal care committee (University of Cologne).

S. Typhimurium infection of macrophages

S. Typhimurium (strain SL1344) was grown to late exponential phase in brain–heart infusion broth at 37°C, and BMDMs were infected with a multiplicity of infection of 10. After 30 min, extracellular bacteria were removed, and macrophages were incubated for 2 h in RPMI medium containing 10% FBS and 50 µg/ml gentamicin. Afterward, macrophages were washed and subsequently cultured in RPMI medium containing 10% FBS and 10 µg/ml gentamicin. At the indicated time points, BMDMs were washed with PBS and collected for experiments.

Bacterial colony formation assay

After 0 and 24 h of infection, BMDMs (0.5×10^6 cells/well) were lysed with 1% Triton X-100 and 0.01% SDS/PBS solution. Lysates were serially diluted with PBS and spread on brain–heart infusion plates, which were incubated overnight at 37°C. The next day, colony-forming units were counted.

Immunoblot analysis

BMDMs ($1.0–2.0 \times 10^6$ cells/well) were lysed with radioimmunoprecipitation assay (RIPA) buffer containing protease and phosphatase

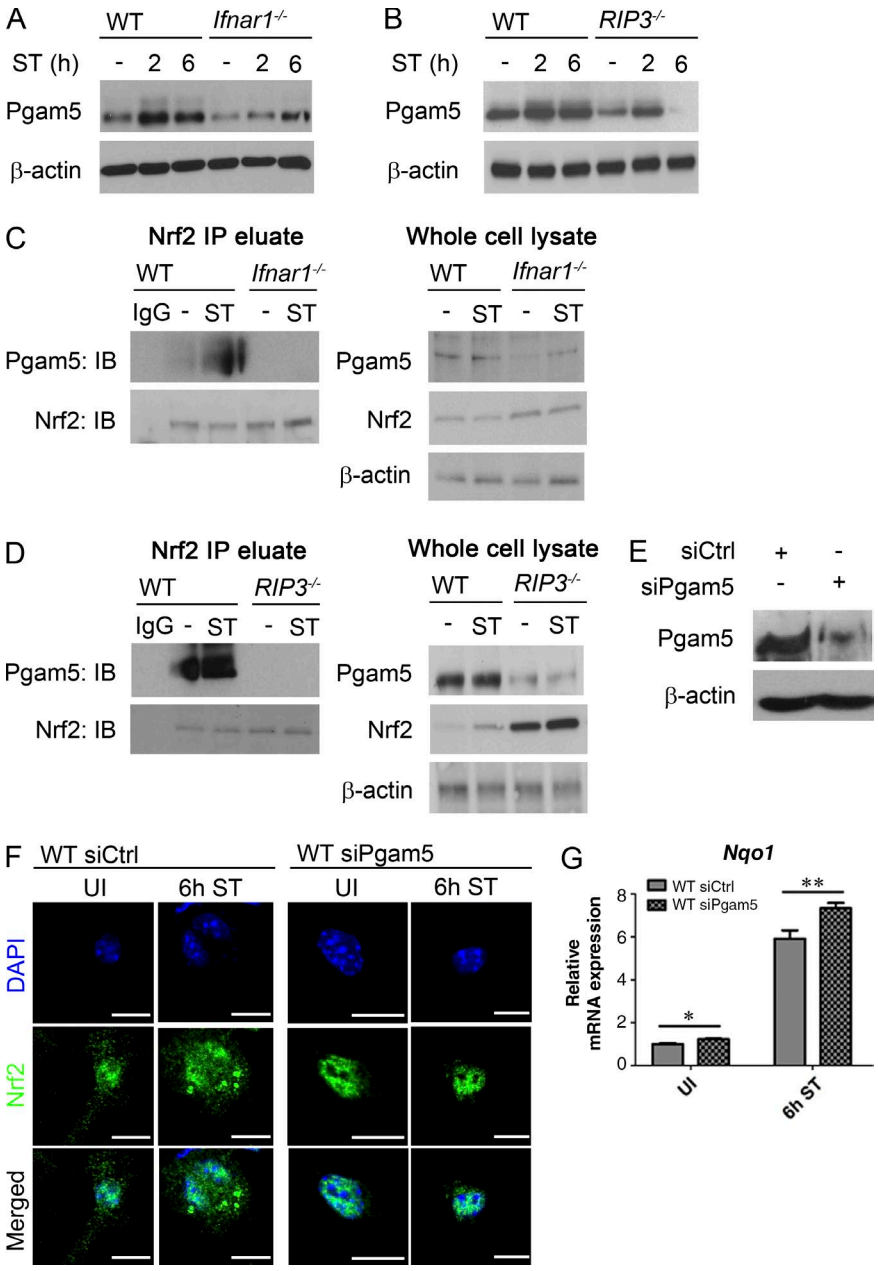

Figure 7. **Pgam5 prevents Nrf2 activation downstream of IFN-I/RIP3.** (A and B) Immunoblot analysis of Pgam5 (B). At the indicated time points, total cell lysates of *S.* Typhimurium–infected WT and *Ifnar1*$^{-/-}$ BMDMs (A) or WT and *RIP3*$^{-/-}$ BMDMs were subjected to SDS-PAGE and were immunoblotted for Pgam5. (C and D) Immunoprecipitation analysis. Anti-Nrf2 immunoprecipitates and total cell lysates from WT and *Ifnar1*$^{-/-}$ BMDMs (C) or WT and *RIP3*$^{-/-}$ BMDMs (D) infected with *S.* Typhimurium for 6 h were analyzed by immunoblot with antibodies against Pgam5 and Nrf2. Samples treated with nonspecific IgG were used as controls. Immunoblots are representative of three independent experiments. (E) Immunoblot analysis of Pgam5 knockdown efficiency. WT BMDMs were transfected with nontargeting (siCtrl) or *Pgam5*-specific siRNA (siPgam5). Thereafter, Pgam5 knockdown efficiency was determined in total cell lysates by immunoblotting. (F) Immunofluorescence staining of nuclear Nrf2. WT BMDMs were transfected with nontargeting (siCtrl) or *Pgam5*-specific siRNA (siPgam5) as described in E. After 6 h of *S.* Typhimurium infection, transfected BMDMs were immunostained for Nrf2, and subcellular localization of Nrf2 was examined by confocal microscopy. Bars, 10 µm. (G) Pgam5-dependent *Nqo1* mRNA expression. Relative mRNA expression levels of *Nqo1* in *S.* Typhimurium–infected WT BMDMs were determined by real-time PCR. Values were normalized to the amounts of mRNA in uninfected BMDMs transfected with siCtrl. Data are means ± SD from three independent experiments with three replicates each. IB, immunoblot. IP, immunoprecipitates. ST, *S.* Typhimurium. UI, uninfected. *, $P < 0.05$; **, $P < 0.01$.

inhibitor cocktail (1861280; Thermo Fisher Scientific). After protein quantification using a bicinchoninic acid protein assay kit (23227; Pierce), equal amounts of protein were resolved by SDS-PAGE, and proteins were transferred to a polyvinylidene difluoride membrane (10600023; GE Healthcare). Next, membranes were blocked with 5% milk in TBS containing 0.05% Tween 20 for 1 h at room temperature and were then incubated overnight at 4°C with primary antibodies against LC3 (L7543; Sigma Aldrich), phospho-p70 S6 kinase (9205; Cell Signaling Technology), p70 S6 kinase (9202; Cell Signaling Technology), SQSTM1/p62 (5114; Cell Signaling Technology), Tom20 (sc-17764; Santa Cruz), Nrf2 (sc-722; Santa Cruz), β-actin (sc-47778; Santa Cruz), Keap1 (10503-2-AP; Proteintech), MLKL (sc-165025, Santa Cruz), phospho-MLKL (ab196436; Abcam), RIP3 (sc-135171; Santa Cruz), phospho-RIP3 (ab195117; Abcam), or Pgam5 (ab126534; Abcam). After washing with TBS–Tween 20, membranes were incubated with the appropriate secondary antibody conjugated to HRP (HAF007 and HAF008; R&D Systems) for 1 h at room temperature. Membranes were washed and incubated with an enhanced chemiluminescence substrate (RPN2106; GE Healthcare) for 1 min and exposed to x-ray film (L-07014-100; Advansta). Densitometric quantification of Western blotting was performed using ImageJ software (National Institutes of Health).

Immunofluorescence staining and confocal microscopy

BMDMs (0.1×10^6 cells/well) were seeded in 24-well plates containing 12-mm round coverslips. After infection, BMDMs were fixed with 4% (wt/vol) formaldehyde in PBS for 15 min at room temperature. BMDMs were washed with PBS and permeabilized with 0.3% Triton X-100 in PBS for 5 min at room temperature. Next, BMDMs were washed with 0.03% Triton X-100 in PBS, followed by incubation with signal enhancer (Image-iT R FX; I36933; Invitrogen) for 30 min and blocking with 5% BSA, 5% goat serum, and 0.03% Triton X-100 in PBS for 1 h at room temperature. After washing, BMDMs were incubated overnight at 4°C with primary antibodies against SQSTM1/p62, Tom20, Nrf2, Keap1, or Pgam5. BMDMs were then washed and incubated with appropriate fluorescent secondary anti-

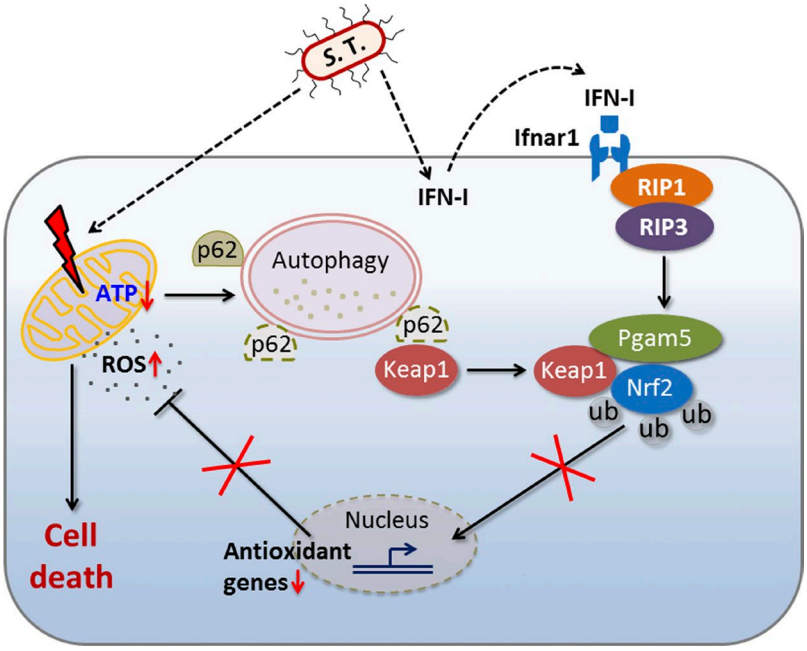

Figure 8. **IFN-I signaling exacerbates mitochondrial damage and cell death by preventing Nrf2-dependent antioxidant response.** *S.* Typhimurium infection induces the para- and autocrine secretion of IFN-I, which subsequently binds to the IFN-I receptor (Ifnar1). In *S.* Typhimurium–infected macrophages, IFN-I induces RIP3-mediated Pgam5 expression. Pgam5 subsequently interacts with Nrf2 (presumably through Keap1), which sequesters Nrf2 in the cytosol, thereby repressing the transcription of Nrf2-dependent antioxidative genes. *S.* Typhimurium–induced oxidative damage results in ROS-mediated mitochondrial dysfunction, energy depletion, transient induction of autophagy, and autophagic degradation of p62. Reduced p62 levels impair interaction of p62 with Keap1, which further decreases Nrf2-dependent antioxidative responses to *S.* Typhimurium infection and sensitizes infected macrophages to cell death. S. T., *S.* Typhimurium. ub, ubiquitin.

bodies (A11008, A11017, and A11072; Invitrogen) for 1 h at room temperature. Coverslips were mounted on glass slides using ProLong gold antifade containing DAPI (P36935; Life Technologies) and stored at 4°C until image acquisition. Images were acquired with a 60× oil Plan Apo objective, numerical aperture 1.4, at room temperature on an inverted confocal microscope (IX81; Olympus) equipped with photomultiplier tube detectors for imaging. Fluoview FV10-ASW 4.2 software (Olympus) was used for acquisition and calculating Pearson's correlation.

Electron microscopy

BMDMs (1.5 × 10^6 cells/well) were fixed (2.5% glutaraldehyde, 2.5% sucrose, 3 mM calcium chloride, and 100 mM Hepes, pH 7.4) for 1 h at room temperature. After washing with 0.1 M cacodylate buffer, pH 7.2, cells were scraped and collected in cacodylate buffer. Cells were centrifuged (for 5 min at 500 *g* and at room temperature) and resuspended in 500 µl of warm 3% low-melting agarose (diluted in cacodylate buffer). Cell suspension was transferred into a sealed 1-ml tip, placed into a 15-ml falcon tube, and centrifuged at 1,500 *g* for 10 min at room temperature to concentrate cells. The agarose pellet was removed from the tip and collected into 0.1 M cacodylate buffer. After fixation, cells were dehydrated in a graded ethanol series (50, 70, 90, and 100%) for 3 min each and were then incubated with ethanol and propylene oxide. Next, cells were embedded using Epon medium. Sections were cut at a thickness of 70 nm (Ultracut UC6; Leica), stained with 1.5% aqueous uranyl acetate for 15 min at 37°C, and contrasted using lead nitrate solution. Samples were examined with an electron microscope (EM109; Zeiss), and images were recorded at 7,000× or 50,000× magnification.

ELISA

Cell culture supernatants from BMDMs (0.5 × 10^6 cells/well) were collected 6 and 24 h after infection and were kept at −80°C until assayed for mouse IL-1β (DY401; R&D Systems) according to the manufacturer's instructions.

Transfection experiments

BMDMs (0.75–1.0 × 10^6 cells/well) were incubated with either 50 nM nontargeting siRNA (SR-CL000-005; Eurogentec) or 50 nM siRNA specific for *Nfe2l2* (Nrf2; L-040766-00-0005; Dharmacon), *Sqstm1* (p62; L-047628-01-0005; Dharmacon), and *Pgam5* (L-052506-01-0005; Dharmacon) together with the transfection reagent Lipofectamine 3000 (L3000-008; Thermo Fisher Scientific) for 48 h according to the manufacturer's instructions. Knockdown efficiency was assessed by Western blot analysis using antibodies against Nrf2, p62, or Pgam5, respectively.

Immunoprecipitation

BMDMs (5.0 × 10^6 cells/well) were lysed with RIPA buffer containing protease and phosphatase inhibitors. After preclearing the cell lysate with protein A/G agarose magnetic beads (16-663; Millipore) for 1 h, beads were removed by placing the tube on a magnetic rack. The whole cell lysate (~500 µg of protein) was incubated with 4 µg of an antibody against Nrf2 overnight at 4°C. Protein A/G agarose beads were added again and incubated for an additional 1 h at room temperature. The immunoprecipitated proteins along with the agarose beads were collected by placing the tube on a magnetic rack. The collected beads were washed several times with RIPA buffer. The washed samples were mixed with SDS-PAGE sample loading buffer, boiled, and resolved on a 10% SDS–polyacrylamide gel. The respective proteins precipitated were identified by immunoblot analysis.

Subcellular fractionation analysis

Nuclear fractions from BMDMs (10^6 cells/well) were prepared using the NE-PER nuclear and cytoplasmic extraction kit (78833; Thermo Fisher Scientific) according to the manufacturer's instructions. Samples were subjected to SDS-PAGE and analyzed by immunoblotting with antibodies against Nrf2, Lamin B (sc-374015; Santa Cruz), and GAPDH (sc-47724; Santa Cruz).

mtROS detection

mtROS was determined with MitoSOX (M36008; Thermo Fisher Scientific) according to the manufacturer's instructions. At the indicated time points, BMDMs (0.5 × 10^6 cells/well) were resuspended in 1% (wt/vol) formaldehyde in PBS. For each experiment, a fluorescence intensity of 50,000 cells was analyzed using a flow cytometer (FACSCanto; Becton Dickinson) and FLOWJO software (Tree Star).

Measurement of ψm

ψm was measured using tetramethylrhodamine methyl ester (TMRM; T-668; Thermo Fisher Scientific). At the indicated time points, the medium was replaced with fresh medium containing 10 µM TMRM, and BMDMs (0.5×10^6 cells/well) were incubated for 10 min at room temperature. Next, cells were washed with PBS, and a fluorescence intensity of 50,000 cells per experiment was analyzed using a FACSCanto flow cytometer and FLOWJO software.

Seahorse assay

OCR was analyzed using the Seahorse XF cell mito stress test kit (Agilent) according to the manufacturer's instructions. In brief, BMDMs were seeded at 0.2×10^5 cells/well in a 96-well Seahorse plate. A utility plate containing equilibration solution (200 µl/well), together with the cartridge, was placed in a CO_2-free incubator at 37°C overnight. The day after, media were removed, and cells were infected with *S.* Typhimurium as described above in *S.* Typhimurium infection of macrophages. 2 h p.i., medium was replaced with glucose, glutamine, and sodium pyruvate–supplemented XF assay buffer (180 µl/well), and the cell culture plate was placed in a CO_2-free incubator for at least 0.5 h. Inhibitors (oligomycin, carbonyl cyanide-4-(trifluoromethoxy) phenylhydrazone, 2DG, and Rotenone) were added to the appropriate port of the injector plate. This plate together with the utility plate was run on the Seahorse analyzer for calibration. Once complete, the utility plate was replaced with the cell culture plate and run on the analyzer (Seahorse XF-96).

ATP measurement

BMDMs (0.1×10^6 cells/well) were plated into a 96-well plate. At the indicated time points, ATP levels were determined using a luminescent cell viability assay (CellTiter-Glo; G7571; Promega) according to the manufacturer's instructions. Luminescence was measured with a multimode plate reader (PerkinElmer).

Cell viability assay

BMDMs (0.1×10^6 cells/well) were plated into a 96-well plate. Cell viability was measured at the indicated time points using lactate dehydrogenase assay (CytoTox 96; G1780; Promega) according to the manufacturer's instructions. Luminescence was measured with a multimode plate reader (PerkinElmer).

Quantitative real-time PCR

Total RNA from BMDMs (10^6 cells/well) was isolated by an RNeasy Mini kit (74106; Qiagen), and 500 ng cDNA was synthesized with random hexamers using reverse transcription (SuperScript III; 18080-044; Invitrogen). Primers (Invitrogen) were designed using Primer3 software and the Basic Local Alignment Search Tool (National Center for Biotechnology Information). 25 µl of PCR reactions contained 10 ng cDNA, 0.4 µmol/liter of each forward and reverse primer, and master mix (SsoFast EvaGreen Supermix; 1725201; Bio-Rad). Real-time PCR was performed under the following conditions: an initial denaturation step of 95°C for 2 min and 40 cycles of 95°C for 5 s and 60°C for 15 s, followed by a denaturation step of 95°C for 60 s and a subsequent melt curve analysis to check amplification specificity. Results were analyzed by the comparative threshold cycle method with hypoxanthine-guanine phosphoribosyltransferase (*Hprt*) as the endogenous reference gene for all reactions. The relative mRNA levels of uninfected BMDMs were used as normalized controls for infected BMDMs. All assays were performed in triplicate, and a nontemplate control was included in all experiments to exclude DNA contamination. Primer sequences are listed in Table 1.

Table 1. **Primer sequences used in this study**

Heading	Sequence (5′ to 3′)
Lc3b (forward)	TCATGGACTGAAGCCAGCATAG
Lc3b (reverse)	TAGCAAAGACAGCTGCATGC
Sqstm1/p62 (forward)	AAACATGGTGCACCCCAATG
Sqstm1/p62 (reverse)	AGATGAGCTTGCTGTGTTCC
Lamp1 (forward)	AGTCTTGTGTTGGCGTTCAG
Lamp1 (reverse)	AGGCAATGCATTACGTGAGC
Nqo1 (forward)	AGCGTTCGGTATTACGATCC
Nqo1 (reverse)	AGTACAATCAGGGCTCTTCTCG
Hmox-1 (forward)	GGTCAGGTGTCCAGAGAAGG
Hmox-1 (reverse)	CTTCCAGGGCCGTGTAGATA
Gclc (forward)	GTGGACGAGTGCAGCAAG
Gclc (reverse)	GTCCAGGAAATACCCCTTCC
Hprt (forward)	GTTGGATACAGGCCAGACTTTGTTG
Hprt (reverse)	GATTCAACTTGCGCTCATCTTAGGC
IL-1β (forward)	GTCCTGTGTAATGAAAGACGGC
IL-1β (reverse)	CTGCTTGTGAGGTGCTGATGTA

Statistical analyses

Data are presented as means ± SD. Statistical analyses were performed using Prism software (version 5; GraphPad). Differences between groups were assessed by two-tailed unpaired Student's *t* test or one-way ANOVA with repeated measures when more than two groups were analyzed. Differences were considered statistically significant when $P \leq 0.05$ (*), very significant when $P \leq 0.01$ (**), and highly significant when $P \leq 0.001$ (***).

Online supplemental material

Fig. S1 depicts OCR in WT and *Ifnar1*$^{-/-}$ BMDMs upon *S.* Typhimurium infection. Fig. S2 A shows p62 expression in *S.* Typhimurium–infected WT BMDMs upon neutralization of IFN-β in comparison with untreated WT and *Atg7*$^{-/-}$ BMDMs. B and C show that differential autophagy levels in WT and *Ifnar1*$^{-/-}$ BMDMs infected with *S.* Typhimurium are not caused by altered mTOR activation and do not affect bacterial burden. Fig. S3 shows that cell death is increased in *S.* Typhimurium–infected *Atg7*$^{-/-}$ BMDMs compared with WT BMDMs, whereas neutralization of IFN-β reduces cell death in both *Atg7*$^{-/-}$ and WT BMDMs. Fig. S4 (A–D) illustrates p62 knockdown efficiency and p62-dependent transcription of Nrf2 downstream genes. E and F show that loss of Atg7 does not affect antioxidative gene expression upon *S.* Typhimurium unless IFN-β is neutralized. Fig. S5 displays *IL-1β* mRNA expression and secretion in *S.* Typhimurium–infected WT and *Ifnar1*$^{-/-}$ BMDMs.

Acknowledgments

We thank the Robinson laboratory members for helpful discussion and Beatrix Martiny from the Cluster of Excellence in Cellular Stress Responses in Aging-associated Diseases (CECAD) Imaging Facility, University of Cologne, for assistance with electron microscopy and Chiara Calabrese from N. Robinson's laboratory for help with confocal microscopy.

This work was supported by funding from the German Center for Infection Research (to N.J. Hos); Center for Molecular Medicine Cologne, University of Cologne (to N.J. Hos and D. Hos); CECAD (funded by the Deutsche Forschungsgemeinschaft within the Excellence Initiative of the German federal and state governments; CECAD grant D01 to N. Robinson); and grants from Deutsche Forschungsgemeinschaft (SFB 670 to N. Robinson and M. Krönke), Köln Fortune, and Maria-Pesch Foundation of the University of Cologne (to N.J. Hos and N. Robinson).

The authors declare no competing financial interests.

Author contributions: N.J. Hos, R. Ganesan, and N. Robinson designed the study and analyzed results. N.J. Hos and R. Ganesan performed experiments. S. Gutiérrez and J. Klimek provided technical assistance and advice. D. Hos performed and analyzed real-time PCRs. Z. Abdullah performed animal breeding and genotyping. N.J. Hos wrote the manuscript with N. Robinson. N. Robinson and M. Krönke conceived and supervised the project. All authors commented on the manuscript, data, and conclusions and approved the final version before submission.

Submitted: 16 January 2017
Revised: 14 July 2017
Accepted: 8 September 2017

References

Arnoult, D., L. Carneiro, I. Tattoli, and S.E. Girardin. 2009. The role of mitochondria in cellular defense against microbial infection. *Semin. Immunol.* 21:223–232. https://doi.org/10.1016/j.smim.2009.05.009

Bjørkøy, G., T. Lamark, A. Brech, H. Outzen, M. Perander, A. Overvatn, H. Stenmark, and T. Johansen. 2005. p62/SQSTM1 forms protein aggregates degraded by autophagy and has a protective effect on huntingtin-induced cell death. *J. Cell Biol.* 171:603–614. https://doi.org/10.1083/jcb.200507002

Chandel, N.S. 2014. Mitochondria as signaling organelles. *BMC Biol.* 12:34. https://doi.org/10.1186/1741-7007-12-34

Denk, H., C. Stumptner, A. Fuchsbichler, T. Müller, G. Farr, W. Müller, L. Terracciano, and K. Zatloukal. 2006. Are the Mallory bodies and intracellular hyaline bodies in neoplastic and non-neoplastic hepatocytes related? *J. Pathol.* 208:653–661. https://doi.org/10.1002/path.1946

Deretic, V., T. Saitoh, and S. Akira. 2013. Autophagy in infection, inflammation and immunity. *Nat. Rev. Immunol.* 13:722–737. https://doi.org/10.1038/nri3532

Ejlerskov, P., J.G. Hultberg, J. Wang, R. Carlsson, M. Ambjørn, M. Kuss, Y. Liu, G. Porcu, K. Kolkova, C. Friis Rundsten, et al. 2015. Lack of Neuronal IFN-β-IFNAR Causes Lewy Body- and Parkinson's Disease-like Dementia. *Cell.* 163:324–339. https://doi.org/10.1016/j.cell.2015.08.069

Galluzzi, L., I. Vitale, J.M. Abrams, E.S. Alnemri, E.H. Baehrecke, M.V. Blagosklonny, T.M. Dawson, V.L. Dawson, W.S. El-Deiry, S. Fulda, et al. 2012. Molecular definitions of cell death subroutines: recommendations of the Nomenclature Committee on Cell Death 2012. *Cell Death Differ.* 19:107–120. https://doi.org/10.1038/cdd.2011.96

Ganesan, R., N.J. Hos, S. Gutierrez, J. Fischer, J.M. Stepek, E. Daglidu, M. Krönke, and N. Robinson. 2017. Salmonella Typhimurium disrupts Sirt1/AMPK checkpoint control of mTOR to impair autophagy. *PLoS Pathog.* 13:e1006227. https://doi.org/10.1371/journal.ppat.1006227

Hara, T., K. Nakamura, M. Matsui, A. Yamamoto, Y. Nakahara, R. Suzuki-Migishima, M. Yokoyama, K. Mishima, I. Saito, H. Okano, and N. Mizushima. 2006. Suppression of basal autophagy in neural cells causes neurodegenerative disease in mice. *Nature.* 441:885–889. https://doi.org/10.1038/nature04724

Ichimura, Y., S. Waguri, Y.S. Sou, S. Kageyama, J. Hasegawa, R. Ishimura, T. Saito, Y. Yang, T. Kouno, T. Fukutomi, et al. 2013. Phosphorylation of p62 activates the Keap1-Nrf2 pathway during selective autophagy. *Mol. Cell.* 51:618–631. https://doi.org/10.1016/j.molcel.2013.08.003

Inami, Y., S. Waguri, A. Sakamoto, T. Kouno, K. Nakada, O. Hino, S. Watanabe, J. Ando, M. Iwadate, M. Yamamoto, et al. 2011. Persistent activation of Nrf2 through p62 in hepatocellular carcinoma cells. *J. Cell Biol.* 193:275–284. https://doi.org/10.1083/jcb.201102031

Ishii, T., K. Itoh, and M. Yamamoto. 2002. Roles of Nrf2 in activation of antioxidant enzyme genes via antioxidant responsive elements. *Methods Enzymol.* 348:182–190. https://doi.org/10.1016/S0076-6879(02)48637-5

Ishimura, R., K. Tanaka, and M. Komatsu. 2014. Dissection of the role of p62/Sqstm1 in activation of Nrf2 during xenophagy. *FEBS Lett.* 588:822–828. https://doi.org/10.1016/j.febslet.2014.01.045

Itakura, E., and N. Mizushima. 2011. p62 Targeting to the autophagosome formation site requires self-oligomerization but not LC3 binding. *J. Cell Biol.* 192:17–27. https://doi.org/10.1083/jcb.201009067

Kelly, B., and L.A. O'Neill. 2015. Metabolic reprogramming in macrophages and dendritic cells in innate immunity. *Cell Res.* 25:771–784. https://doi.org/10.1038/cr.2015.68

Kobayashi, A., M.I. Kang, H. Okawa, M. Ohtsuji, Y. Zenke, T. Chiba, K. Igarashi, and M. Yamamoto. 2004. Oxidative stress sensor Keap1 functions as an adaptor for Cul3-based E3 ligase to regulate proteasomal degradation of Nrf2. *Mol. Cell. Biol.* 24:7130–7139. https://doi.org/10.1128/MCB.24.16.7130-7139.2004

Komatsu, M., S. Waguri, T. Chiba, S. Murata, J. Iwata, I. Tanida, T. Ueno, M. Koike, Y. Uchiyama, E. Kominami, and K. Tanaka. 2006. Loss of autophagy in the central nervous system causes neurodegeneration in mice. *Nature.* 441:880–884. https://doi.org/10.1038/nature04723

Komatsu, M., S. Waguri, M. Koike, Y.S. Sou, T. Ueno, T. Hara, N. Mizushima, J. Iwata, J. Ezaki, S. Murata, et al. 2007. Homeostatic levels of p62 control cytoplasmic inclusion body formation in autophagy-deficient mice. *Cell.* 131:1149–1163. https://doi.org/10.1016/j.cell.2007.10.035

Komatsu, M., H. Kurokawa, S. Waguri, K. Taguchi, A. Kobayashi, Y. Ichimura, Y.S. Sou, I. Ueno, A. Sakamoto, K.I. Tong, et al. 2010. The selective autophagy substrate p62 activates the stress responsive transcription factor Nrf2 through inactivation of Keap1. *Nat. Cell Biol.* 12:213–223.

Kroemer, G., L. Galluzzi, and C. Brenner. 2007. Mitochondrial membrane permeabilization in cell death. *Physiol. Rev.* 87:99–163. https://doi.org/10.1152/physrev.00013.2006

Lau, A., X.J. Wang, F. Zhao, N.F. Villeneuve, T. Wu, T. Jiang, Z. Sun, E. White, and D.D. Zhang. 2010. A noncanonical mechanism of Nrf2 activation by autophagy deficiency: direct interaction between Keap1 and p62. *Mol. Cell. Biol.* 30:3275–3285. https://doi.org/10.1128/MCB.00248-10

Lewis, J.A., A. Huq, and P. Najarro. 1996. Inhibition of mitochondrial function by interferon. *J. Biol. Chem.* 271:13184–13190. https://doi.org/10.1074/jbc.271.22.13184

Lindgren, S.W., I. Stojiljkovic, and F. Heffron. 1996. Macrophage killing is an essential virulence mechanism of Salmonella typhimurium. *Proc. Natl. Acad. Sci. USA.* 93:4197–4201. https://doi.org/10.1073/pnas.93.9.4197

Lo, S.C., and M. Hannink. 2006. PGAM5, a Bcl-XL-interacting protein, is a novel substrate for the redox-regulated Keap1-dependent ubiquitin ligase complex. *J. Biol. Chem.* 281:37893–37903. https://doi.org/10.1074/jbc.M606539200

Lo, S.C., and M. Hannink. 2008. PGAM5 tethers a ternary complex containing Keap1 and Nrf2 to mitochondria. *Exp. Cell Res.* 314:1789–1803. https://doi.org/10.1016/j.yexcr.2008.02.014

Man, S.M., R. Karki, B. Briard, A. Burton, S. Gingras, S. Pelletier, and T.D. Kanneganti. 2017. Differential roles of caspase-1 and caspase-11 in infection and inflammation. *Sci. Rep.* 7:45126. https://doi.org/10.1038/srep45126

Mathew, R., C.M. Karp, B. Beaudoin, N. Vuong, G. Chen, H.Y. Chen, K. Bray, A. Reddy, G. Bhanot, C. Gelinas, et al. 2009. Autophagy suppresses tumorigenesis through elimination of p62. *Cell.* 137:1062–1075. https://doi.org/10.1016/j.cell.2009.03.048

Meunier, E., M.S. Dick, R.F. Dreier, N. Schürmann, D. Kenzelmann Broz, S. Warming, M. Roose-Girma, D. Bumann, N. Kayagaki, K. Takeda, et al. 2014. Caspase-11 activation requires lysis of pathogen-containing vacuoles by IFN-induced GTPases. *Nature.* 509:366–370. https://doi.org/10.1038/nature13157

Mizushima, N., B. Levine, A.M. Cuervo, and D.J. Klionsky. 2008. Autophagy fights disease through cellular self-digestion. *Nature.* 451:1069–1075. https://doi.org/10.1038/nature06639

Olagnier, D., S. Peri, C. Steel, N. van Montfoort, C. Chiang, V. Beljanski, M. Slifker, Z. He, C.N. Nichols, R. Lin, et al. 2014. Cellular oxidative stress response controls the antiviral and apoptotic programs in dengue virus-infected dendritic cells. *PLoS Pathog.* 10:e1004566. https://doi.org/10.1371/journal.ppat.1004566

Owen, K.A., C.B. Meyer, A.H. Bouton, and J.E. Casanova. 2014. Activation of focal adhesion kinase by Salmonella suppresses autophagy via an Akt/mTOR signaling pathway and promotes bacterial survival in macrophages. *PLoS Pathog.* 10:e1004159. https://doi.org/10.1371/journal.ppat.1004159

Pankiv, S., T.H. Clausen, T. Lamark, A. Brech, J.A. Bruun, H. Outzen, A. Øvervatn, G. Bjørkøy, and T. Johansen. 2007. p62/SQSTM1 binds directly to Atg8/LC3 to facilitate degradation of ubiquitinated protein aggregates by autophagy. *J. Biol. Chem.* 282:24131–24145. https://doi.org/10.1074/jbc.M702824200

Robinson, N., S. McComb, R. Mulligan, R. Dudani, L. Krishnan, and S. Sad. 2012. Type I interferon induces necroptosis in macrophages during infection with Salmonella enterica serovar Typhimurium. *Nat. Immunol.* 13:954–962. https://doi.org/10.1038/ni.2397

Rubinsztein, D.C. 2006. The roles of intracellular protein-degradation pathways in neurodegeneration. *Nature.* 443:780–786. https://doi.org/10.1038/nature05291

Rushmore, T.H., M.R. Morton, and C.B. Pickett. 1991. The antioxidant responsive element. Activation by oxidative stress and identification of the DNA consensus sequence required for functional activity. *J. Biol. Chem.* 266:11632–11639.

Schmeisser, H., S.B. Fey, J. Horowitz, E.R. Fischer, C.A. Balinsky, K. Miyake, J. Bekisz, A.L. Snow, and K.C. Zoon. 2013. Type I interferons induce autophagy in certain human cancer cell lines. *Autophagy.* 9:683–696. https://doi.org/10.4161/auto.23921

Stavru, F., F. Bouillaud, A. Sartori, D. Ricquier, and P. Cossart. 2011. Listeria monocytogenes transiently alters mitochondrial dynamics during infection. *Proc. Natl. Acad. Sci. USA.* 108:3612–3617. https://doi.org/10.1073/pnas.1100126108

Stumptner, C., A. Fuchsbichler, K. Zatloukal, and H. Denk. 2007. In vitro production of Mallory bodies and intracellular hyaline bodies: the central role of sequestosome 1/p62. *Hepatology.* 46:851–860. https://doi.org/10.1002/hep.21744

Thompson, H.G., J.W. Harris, B.J. Wold, F. Lin, and J.P. Brody. 2003. p62 overexpression in breast tumors and regulation by prostate-derived Ets factor in breast cancer cells. *Oncogene.* 22:2322–2333. https://doi.org/10.1038/sj.onc.1206325

Thurston, T.L., S.A. Matthews, E. Jennings, E. Alix, F. Shao, A.R. Shenoy, M.A. Birrell, and D.W. Holden. 2016. Growth inhibition of cytosolic Salmonella by caspase-1 and caspase-11 precedes host cell death. *Nat. Commun.* 7:13292. https://doi.org/10.1038/ncomms13292

Umemura, A., F. He, K. Taniguchi, H. Nakagawa, S. Yamachika, J. Font-Burgada, Z. Zhong, S. Subramaniam, S. Raghunandan, A. Duran, et al. 2016. p62, Upregulated during Preneoplasia, Induces Hepatocellular Carcinogenesis by Maintaining Survival of Stressed HCC-Initiating Cells. *Cancer Cell.* 29:935–948. https://doi.org/10.1016/j.ccell.2016.04.006

Wang, Z., H. Jiang, S. Chen, F. Du, and X. Wang. 2012. The mitochondrial phosphatase PGAM5 functions at the convergence point of multiple necrotic death pathways. *Cell.* 148:228–243. https://doi.org/10.1016/j.cell.2011.11.030

Wasilewski, M., and L. Scorrano. 2009. The changing shape of mitochondrial apoptosis. *Trends Endocrinol. Metab.* 20:287–294. https://doi.org/10.1016/j.tem.2009.03.007

Wasserman, W.W., and W.E. Fahl. 1997. Functional antioxidant responsive elements. *Proc. Natl. Acad. Sci. USA.* 94:5361–5366. https://doi.org/10.1073/pnas.94.10.5361

Weinberg, S.E., L.A. Sena, and N.S. Chandel. 2015. Mitochondria in the regulation of innate and adaptive immunity. *Immunity.* 42:406–417. https://doi.org/10.1016/j.immuni.2015.02.002

Zatloukal, K., C. Stumptner, A. Fuchsbichler, H. Heid, M. Schnoelzer, L. Kenner, R. Kleinert, M. Prinz, A. Aguzzi, and H. Denk. 2002. p62 Is a common component of cytoplasmic inclusions in protein aggregation diseases. *Am. J. Pathol.* 160:255–263. https://doi.org/10.1016/S0002-9440(10)64369-6

Zhang, D.D., S.C. Lo, J.V. Cross, D.J. Templeton, and M. Hannink. 2004. Keap1 is a redox-regulated substrate adaptor protein for a Cul3-dependent ubiquitin ligase complex. *Mol. Cell. Biol.* 24:10941–10953. https://doi.org/10.1128/MCB.24.24.10941-10953.2004